*AAPS PharmSciTech (2019) 20: 47*
DOI: 10.1208/s12249-018-1260-4

*Research Article*

*Theme: Advancements in Dissolution Testing of Oral and Non-Oral Formulations*
*Guest Editor: Sandra Klein*

# Understanding the Potential for Dissolution Simulation to Explore the Effects of Medium Viscosity on Particulate Dissolution

**Deirdre M. D'Arcy[1,3] and Tim Persoons[2]**

*Received 28 June 2018; accepted 24 November 2018; published online 7 January 2019*

***Abstract.*** Viscosity, influenced by medium composition, will affect the hydrodynamics of a dissolution system. Dissolution simulation methods are valuable tools to explore mechanistic dissolution effects, with an understanding of limitations of any simulation method essential to its appropriate use. The aims of this paper were a) to explore, using dissolution simulation, the effects of slightly viscous media on particulate dissolution and b) to illustrate approaches to, and limitations of, the dissolution simulations. A lumped parameter fluid dynamics dissolution simulation model (SIMDISSO™) was used to simulate particulate (20 and 200 μm diameter) dissolution in media with viscosity at 37 °C of water (0.7 mPa.s), milk (1.4 mPa.s) and a nutrient drink (12.3 mPa.s). Effects of flow rate, modality (constant *vs* pulsing), viscosity and gravitational and particle motion/sedimentation effects on simulated dissolution were explored, in the flow through and paddle apparatuses as appropriate. Shadowgraph imaging (SGI) was used to visualise particle suspension behaviour. Flow rate, hydrodynamic viscous effects and disabling particle motion and gravitational effects affected simulated dissolution of larger particles. SGI imaging revealed retention of particles in suspension in 1.4 mPa.s medium, which sedimented in water. The effect of diffusion adjusted for viscosity was significant for both particle sizes. The limitations of this 1D simulation approach would be greater for larger particles in low velocity regions of the paddle apparatus. Even slightly viscous media can affect dissolution of larger particles with dissolution simulation affording insight into the mechanisms involved, provided the assumptions and limitations of the simulation approach are clarified and understood.

**KEY WORDS:** dissolution simulation; fluid dynamics; viscosity; particle dissolution; modelling and simulation.

## INTRODUCTION

Recent advances in dissolution science include hydrodynamic measurements and simulations (1), more detailed categorisation of biorelevant dissolution media (2,3), novel apparatus design to replicate more closely the gastrointestinal environment (4,5) and an increasing capacity for in-depth *in silico* dissolution modelling. These developments have occurred against the background of the rapidly evolving field of physiologically based pharmacokinetic (PBPK) modelling. In the field of biopharmaceutics, it is attempted to address the challenge of bridging *in vitro* dissolution testing and PBPK through development of *in vivo* predictive dissolution (IPD) testing. The *in vivo* gastrointestinal environment is recognised as having many sources of variability, from luminal media composition (6–8) and physicochemical variation (9–11) to hydrodynamic considerations such as intestinal liquid distribution and pressures (12,13). Consequently, *in vitro* dissolution test conditions are continuously being developed to facilitate more biorelevant dissolution environments for IPD. As increasing efforts are being made to replicate some of these properties in *in vitro* dissolution testing, it is crucial to maintain a mechanistic understanding of the impact of the dissolution environment on the dissolution rate. There is now a significant body of literature available detailing fluid dynamic simulations and velocimetric measurements to characterise hydrodynamics in the paddle, basket, reciprocating cylinder and flow through apparatuses (1,14,15), along with a growing body of *in silico* simulation studies aiming to characterise the gastrointestinal hydrodynamic environment (16–20).

Guest Editor: Sandra Klein

[1] School of Pharmacy and Pharmaceutical Sciences, Trinity College Dublin, Dublin 2, Ireland.
[2] Department of Mechanical and Manufacturing Engineering, Trinity College Dublin, Dublin 2, Ireland.
[3] To whom correspondence should be addressed. (e–mail: ddarcy@tcd.ie)

Whereas, consensus has evolved concerning the categorisation and composition of various types of biorelevant dissolution media in *in vitro* dissolution testing, a biorelevant *in vitro* hydrodynamic environment is less well defined. Nonetheless, agitation conditions and hydrodynamic variability can affect dissolution rates, and a greater understanding of hydrodynamic conditions in the dissolution apparatuses supports interpretation of dissolution data generated. However, hydrodynamics can be interpreted as relating to agitation conditions, and thus sometimes interpreted as an aspect of dissolution test conditions separate to media composition. Media composition can affect fluid density and, in particular, viscosity, which can notably affect the hydrodynamic environment.

Currently, biorelevant media are defined as a hierarchy with four levels of complexity (2). Viscosity is presented as being relevant to the most complex level and it is relevant in particular to conditions representing the fed stomach and the lower intestine. Fed stomach contents would be expected to be highly viscous (21,22) based on observed viscosity values of a standard FDA meal. Whereas, the viscosity of an FDA meal (diluted to 900 mL) was 467 ± 100 mPa.s, even orange juice with an observed viscosity of 3.37 mPa.s is several times more viscous than water at 37 °C (0.7 mPa.s) (23) (22), as are fasted state gastric aspirate fluids (range 1.7–9.3 mPa.s (6)). The potential small increases in viscosity relative to simple buffer systems, from media used to represent the fed gastric state without necessarily aiming to replicate *in vivo* viscosities, could affect hydrodynamics and therefore dissolution. Milk, which has been investigated as a single or major component of the dissolution medium (3,8,24) with relevance in particular for, for example, the early post-prandial phase in the infant population (3), has a viscosity of approximately 1.4 mPa.s, double that of water at 37 °C. The main focus of the current work was to explore, through dissolution simulation using a fluid dynamics mass transfer model (25,26), the effects of viscosity on simulated particulate dissolution. Dissolution in media with viscosity values representing water, milk and a food supplement (Ensure plus® (21)) were simulated in the paddle and flow through apparatuses (USP apparatus 2 and 4, respectively (27)), along with some dissolution imaging results illustrating the effect on particle motion of a small increase in viscosity of the dissolution medium. A range of simulation options to represent the dissolution environment in a lumped parameter model with a unidirectional velocity field were employed.

A secondary focus of the current work was to present approaches and limitations to *in silico* simulation of particulate dissolution in different apparatuses (the paddle and flow through dissolution apparatuses), with a focus on consideration of the spatial limitations of the dissolution environment, the simulation of a pulsing *vs.* constant flow, and the inclusion of gravitational effects.

Advances in computer technology have enabled access to considerable computational capacity even on a standard PC/laptop, facilitating use of simulation technology to investigate many complex cause-effect relationships. As *in silico* modelling and simulation now represent a valuable core tool in the development of IPD, it is also critical that the strengths and limitations of any particular simulation approach are understood. For example, in dissolution simulation, is the 3D spatial environment simulated, are gravitational effects included, is particle motion accounted for in the relative fluid velocity parameter, is the simulation time-varying or representing a steady state? Increasing the complexity of a simulation should increase its accuracy, but the computational resources required for such increased complexity might represent an undesirable, and unnecessary, cost. Ultimately every simulation will include assumptions and limitations, and understanding the simulation limitations will aid interpretation of the results, adding confidence and value to the role of *in silico* simulation in IPD.

## METHODS

### Dissolution Simulations and Theoretical Basis

The dissolution simulations were carried out using in-house *in vitro* dissolution simulation software (SIMDISSO™). The methods used, employing a lumped parameter fluid dynamics-based mass transfer model, have been previously described (26). Simulations were solved using Matlab (The MathWorks, Natick Massachusetts, USA), using the 'ode15s' variable time step solver. This method has been shown to perform well in predicting dissolution of non-agglomerating particulate systems in the flow-through apparatus with the cell-size used in the current work (26,28). Variables being solved in the lumped parameter model include particle diameter, $d_p$, cell concentration ($C_c$) and reservoir concentration ($C_r$). To facilitate better replication of the local near-particle environment, an option of another user-defined parameter was introduced to describe available local volume ($V_b$) for the dissolving particle, scaled to the particle radius. Total $V_b$ cannot exceed the cell volume. $C_b$, the bulk concentration in $V_b$, is a further variable solved. (Paddle apparatus simulations combine cell and reservoir volumes for vessel volume).

In brief, the following steps were undertaken in each time step (0.001 s):

Step 1

Using known inputs of particle density ($\rho_p$), initial $d_p$ and initial mass to be dissolved, the number of particles present in the system was calculated.

Step 2

The Reynolds number, Re, which relates dimensions, density, velocity and viscosity, was solved using Eq. 1. Initial $d_P$, fluid density ($\rho_f$) and dynamic viscosity ($\mu_f$) were input to the simulation model, along with fluid velocity, which was input as an oscillating semi-sinusoidal velocity profile (pulsing flow through cell) or a constant velocity (flow through cell without pulse or paddle apparatus configuration):

$$Re = \rho_f |U_f - U_p| d_p / \mu_f \quad (1)$$

where $U_f$ is the fluid velocity and $U_p$ is the particle velocity.

In Eq. 1, if particle motion is disabled, the particle is static, particle motion ($U_p$) is zero and the relevant fluid velocity term is the absolute velocity, $U_f$.

If particle motion is enabled, the relevant velocity term is the relative fluid velocity (the difference between fluid and particle velocities), represented in Eq. 1 by $|U_f - U_p|$.

When particle motion was enabled, the $U_p$ value in Eq. 1 was calculated using the particle size at each time step (reducing as the particle dissolves), by the following:

$$m_p \frac{dU_p}{dt} = F_{drag} + F_{buoy} + F_{fluid\ acc} + F_{Basset} \quad (2)$$

where $F_{drag}$, $F_{buoy}$, $F_{fluid\ acc}$ and $F_{Basset}$ are the drag, buoyancy, fluid acceleration and (negligible) Basset history integral forces, respectively, acting on the particle. The term $m_p$ represents the apparent particle mass, which includes a contribution from the adjacent fluid mass for the calculation of particle motion (26).

Step 3

The value of Re from Eq. 1 was used to simulate mass transfer, and thus dissolution rate, through calculation of the mass transfer coefficient, k, *via* the Sherwood number (Sh); Sh can be defined as $\frac{kd_p}{D}$, where $D$ is the diffusion coefficient (known value for $D$ is input in the simulation model, with the $d_p$ value reducing with each time step as the particle dissolves). Sh is related to Re and the Schmidt number (Sc), using the Ranz Marshall correlation (29), as follows:

$$Sh = 2 + 0.6Re^{1/2}Sc^{1/3} \quad (3)$$

where Sc is defined as $\frac{v_f}{D}$, $v_f$ being the kinematic viscosity, thus relating momentum and mass diffusivity.

Equation 3 can also be written as:

$$\frac{k\,d_p}{D} = 2 + 0.6\left(\frac{|U_f - U_p|d_p}{v_f}\right)^{\frac{1}{2}}\left(\frac{v_f}{D}\right)^{\frac{1}{3}} \quad (4)$$

Step 4

The mass transfer coefficient, calculated from Eq. 4, was used to estimate the change in particle diameter with time, through the following relationship:

$$\frac{d(d_p)}{dt} = -k.\frac{2(C_s - C_b)}{\rho_p} \quad (5)$$

where $C_s$ is the solubility.

Step 5

Estimation of the change in individual $d_p$ with time from step 4, along with the total particle number and particle density, allows simulation of total mass dissolved with time.

Step 6

The total mass dissolved in each time step affects $C_c$, which is also modulated by the flow through the cell over each time step; $C_c$ along with the flow rate and reservoir volume determine $C_r$. $C_b$ and thus the concentration gradient in Eq. 5, varies with inlet concentration ($C_r$ in closed system), flow rate, mass dissolved and $V_b$.

In terms of particle motion, gravitational effects are relevant to $F_{buoy}$, and viscosity to $F_{drag}$ in Eq. 2. Re decreases with increased viscosity, as evidenced by the presence of $\mu_f$ as the denominator in Re (Eq. 1). Furthermore, if particle motion is enabled, increased viscosity will decrease Re through increased drag (Eq. 2) and therefore reduced relative velocity value, $U_f - U_p$. On the contrary, an increase in $v_f$, with a corresponding decrease in $D$, will lead to an increase in Sc, having a positive effect on the dissolution rate. As evident in Eq. 4, this positive effect on Sc is outweighed by the negative effects of viscosity on Re and Sh. Ultimately, considering Eqs. 2–4, increasing viscosity should decrease the dissolution rate. However, considering these equations in abstract without considering the spatial environment of the dissolution test can be misleading, as viscosity can also affect particle sedimentation behaviour and thus the dissolution environment the particle is exposed to.

## Limitations and Assumptions in the Model

The main assumptions of the model were (i) of rigid spherical, particles; (ii) that there was no interaction between particles (besides concentration being affected by total mass dissolved from all particles); (iii) of a uniform and unidirectional velocity field.

The lumped parameter model does not include a hydrodynamic simulation (apart from the input flow profile); therefore, the effect of reservoir/vessel dimensions was limited to concentration effects on simulated dissolution rate. As the primary flow direction in the paddle apparatus occurs in the horizontal plane, gravitational effects in this unidirectional model could not be included in the paddle apparatus simulations. Table I further outlines the relevance of the model and its approximations to the real operational configuration of the dissolution apparatuses considered in the simulations.

## Properties Investigated

The reference case employed in the simulations (Table II) was a 200-μm diameter particle, solubility 0.23 mg $mL^{-1}$, diffusion coefficient ($D$) of $8.7 \times 10^{-10}$ $m^2$ $s^{-1}$, using the flow through apparatus (12 mm diameter cell) with a reservoir volume of 250 mL and a pulsing flow mode. These are conditions relevant to, for example, carbamazepine (CBZ) particulate dissolution (30,31).

An initial drug mass of 20 mg was used for all simulations.

Simulations were also carried out in an environment representing the paddle apparatus (900 mL) with velocity values taken from ultrasound-pulse-echo data (32,33) and CFD simulations (34,35), representing an approximate range of fluid velocity magnitudes at the centre of the base of the paddle apparatus at 25–50 rpm (0.0024 $ms^{-1}$) and at the top of a tablet located at the centre of the vessel base at 50 rpm (0.05 $ms^{-1}$). The properties investigated in the simulations (Table II) include flow rate, viscosity, flow modality (pulsing/

**Table I.** Relevance of simulation approximations and limitations to the respective dissolution apparatuses

| | Particle dissolution characteristics | Flow profile | Gravitational force | Spatial consideration | Factors affecting concentration |
|---|---|---|---|---|---|
| Flow-through apparatus | Uniform, rigid, spherical particles. Particle size (or size distribution) and density defined. Dissolution occurs into defined volume ($V_b$) surrounding each particle—this volume cannot exceed the cell volume. Can be defined as total cell volume or scaled to the particle radius | Unidirectional, constant or pulsing flow; Unidirectional flow representative of dominant vertical flow operational characteristics of the apparatus. | Enabled or disabled; direction of flow (vertical upward) facilitates inclusion of the countering effect of gravity. | Can disable particle motion if vertical particle motion simulation suggests particle will be halted by upper/lower cell boundary; Facilitates consideration of spatial limitations of apparatus. | Concentration gradient driving dissolution affected by dissolution rate, flow rate through cell and cell size, reservoir size, inlet concentration (open system: concentration zero at inlet; closed system: inlet concentration equal to reservoir concentration); and $V_b$. |
| Paddle apparatus | (in the current work $V_b$ defined as extending 3 radii from particle surface))* | Unidirectional, constant. Flow velocity representative of velocity magnitudes in the apparatus, without accounting for direction. | Inappropriate to enable as flow not defined as vertical, thus gravitational effects not simulated. | Can disable particle motion if particle characteristics suggest they are not likely to be carried in the flow. Due to the complexity of the apparatus hydrodynamics, this relates to particle motion properties rather than spatial limitations of apparatus. | Assumes immediate distribution of local dissolved mass into the vessel volume. Concentration gradient affected by dissolution rate, fluid velocity, reservoir (vessel) concentration and $V_b$. |

*The definition of the local volume ($V_b$) surrounding the particle is semi-empirical, and the model choices provide the user with the option to define the volume which reflects the observed particulate behaviour i.e. for more concentrated well dispersed particulate systems, the volume can be the total cell volume/particle number. In the more likely scenario of more dilute systems remaining in e.g. the lower region of the cell, the volume can be defined as scaled to the particle radius to reflect more limited exposure to the dissolution medium in the cell.

constant) and the *D* value; along with variation in particle motion:

(Particle motion enabled: relative velocity used to calculate Re in SIMDISSO™ (Eq. 1); particle motion disabled (static particle): absolute velocity used to calculate Re in SIMDISSO™ (Eq. 1)).

The viscosity values used represent the following: level 1 (0.7 mPa.s), water at 37 °C (23); level 2 (1.4 mPa.s), milk at 37 °C, (21) (1.5 mPa.s), (36)(1.3 mPa.s); level 3 (12.3 mPa.s), nutrient feed Ensure Plus ® at 37 °C (21).

When the *D* value was adjusted for viscosity, this was done based on the Stokes-Einstein equation, where *D* is proportional to the reciprocal of viscosity.

"*D* unadjusted" refers to the situation in the simulation where the fluid viscosity is level 2 or 3, but the *D* value is retained at the reference value, level 1, representing media where the *D* is not altered by increased viscosity (*e.g.* some polymeric solutions). "*D* adjusted" refers to the *D* value being adjusted appropriate to the relevant fluid viscosity.

## Shadowgraph Imaging

Shadowgraph imaging (SGI) was conducted as previously described (26), with the exceptions of an LED light source being used in place of a laser, camera a Grasshopper 3 GS3-U3-23S6c (Point Grey Research), and in-house code used to determine particle dimensions. Fifteen seconds of video were recorded at each dissolution sampling time, with a 10-Hz frame rate. In brief, 20 mg CBZ powder (Sigma) were used in the flow through apparatus (Sotax CE1, 12 mm cell, 250 mL reservoir volume, 8 mL $min^{-1}$, closed loop). Media used were degassed water (viscosity 0.7 mPa.s) and 0.3% *w/v* HPMC solution (viscosity 1.37 mPa.s) (H9262, Sigma). Due to the low concentration and grade of HPMC used, Newtonian behaviour was assumed. Viscosity was measured using Vibro SV-10 viscometer (A and D company Ltd.) ($n = 3$). CBZ particle size was measured using a Malvern Mastersizer 2000 (Hydro μP, dispersant water) ($n = 3$); the d50 value was 262 μm.

SGI facilitates a quantitative analysis of particle numbers and size, present in the imaging window (approximately the centre portion of the cell) (26,28). The image sequences presented were recorded at 10, 20 and 30 min after the beginning of the dissolution test.

## RESULTS

This section is presented as a series of simulated dissolution results progressing from the reference case in the flow through apparatus, exploring effects of flow rate, viscosity and particle motion through to the effect of flow modality (constant *vs* pulsing) and gravitational effects. Thereafter, the simulation evolves through changing cell/reservoir volume, while maintaining constant flow and disabling gravitational acceleration, thus finally presenting results from the paddle apparatus simulations.

## Flow Through Apparatus

### *Effect of Viscosity and Flow Rate (Particle Motion Enabled)*

The effects of flow rate and viscosity on simulated dissolution rates (200 μm diameter particles), with particle

**Table II.** Dissolution system parameters investigated in the dissolution simulations. (reference conditions italicized). Viscosity values as indicated are referred to as levels 1–3 throughout the manuscript

| Viscosity (mPa.s) | Flow rate for pulsing flow (mL $min^{-1}$) | Flow through apparatus velocity without pulse (m $s^{-1}$) | Solubility (mg $mL^{-1}$) | Particle size (m) | Diffusion coefficient (D) ($m^2$ $s^{-1}$) | Particle motion | Gravitational force | Reservoir volume (mL) | Paddle apparatus velocity (m $s^{-1}$) |
|---|---|---|---|---|---|---|---|---|---|
| *0.7 (Level 1)* | *8* | 0.0012 (8 mL $min^{-1}$) | *0.23* | *$200 \times 10^{-6}$* | *$8.7 \times 10^{-10}$* | *Enabled* | *Enabled* | Flow through apparatus: *250* | 0.0024 |
| 1.4 (Level 2) | 16 | 0.0024 (16 mL $min^{-1}$) | 0.02 | $20 \times 10^{-6}$ | $4.38 \times 10^{-10}$ | Disabled | Disabled | Paddle apparatus: 900 | 0.05 |
| 12.3 (Level 3) | | | | | $0.495 \times 10^{-10}$ | | | | |

motion enabled, are illustrated in Fig. 1. A small change in viscosity from level 1 to level 2 had a greater impact on dissolution rate than the effect of flow rate, even when *D* was not adjusted for viscosity. The effect was similar when dissolution was slower due to lower solubility (Fig. 1b).

With *D* adjusted for viscosity, the effect of viscosity on dissolution was more pronounced, the effect of flow rate less notable and the dissolution rate much reduced (Fig. 2).

### *Effect of Particle Size*

Figure 3 shows the simulated dissolution of 20 μm diameter particles. As expected, the dissolution rate was much higher than for the 200 μm particles, but the flow rate was associated with a greater effect for the 20 μm particles. There was no observable effect on dissolution from viscosity when *D* was unadjusted, however with *D* adjusted for viscosity, the effect of viscosity on diffusion dominated, with the overall dissolution rate much lower.

Therefore, the hydrodynamic effect of viscosity was more relevant for larger particles, but the effect of viscosity on diffusion was notable for both particle sizes.

### *Simulated Particle Velocities and Motion*

When particle motion was enabled, Re (Eq. 1) was based on the relative velocity, *i.e.* ($U_f$ − $U_p$). Figure 4 illustrates the simulated fluid and particle velocity in level 1 and 3 viscosity medium, at both 8 and 16 mL $min^{-1}$. The relative velocity was similar at both flow rates for any given viscosity for both particle sizes (*e.g.* Figure 4a *vs.* b, e *vs.* f). For the 200 μm particles, the relative velocity decreased as the viscosity increased (*e.g.* Fig. 4a *vs* c), but for the smaller 20 μm particles, neither viscosity nor flow rate substantially affected the relative velocity value (Fig. 4e–h). Although the relative velocity at each flow rate was similar, in

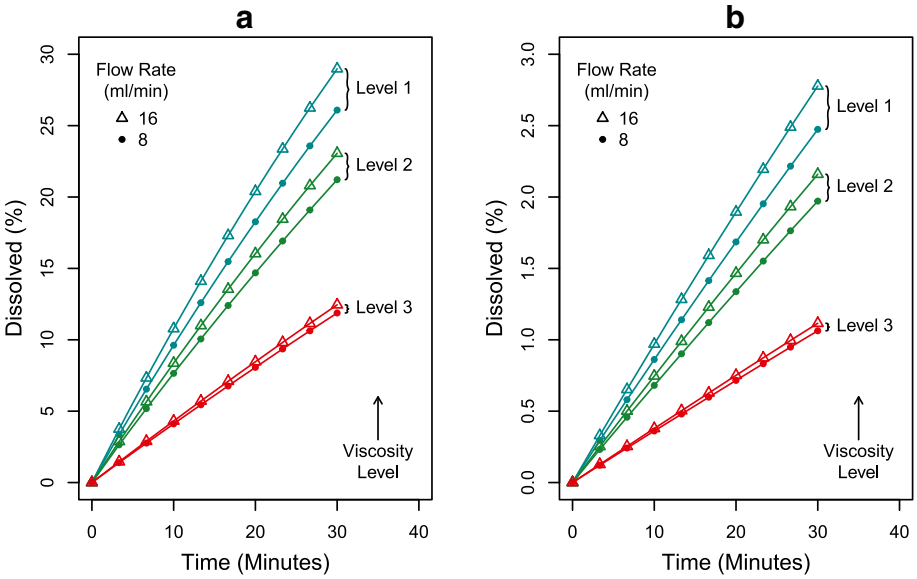


**Fig. 1.** Effect of flow rate and viscosity (*D* unadjusted) on simulated dissolution of 200 μm diameter particles. **a**: solubility 0.23 mg $mL^{-1}$, **b**: solubility 0.02 mg $mL^{-1}$. Levels 1–3 refer to viscosity 0.7 mPa.s, 1.4 mPa.s and 12.3 mPa.s respectively

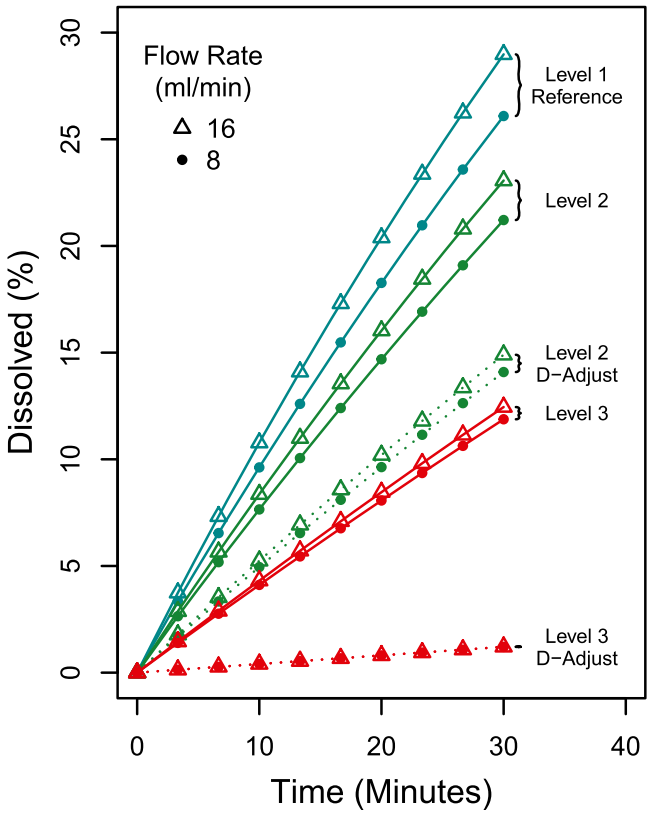


**Fig. 2.** Effect of adjusting diffusion coefficient for viscosity on simulated dissolution of 200 μm diameter particles, solubility 0.23 mg $mL^{-1}$. Levels 1–3 refer to viscosity 0.7 mPa.s, 1.4 mPa.s and 12.3 mPa.s respectively. *D*-adjust refers to the simulated dissolution profile when the diffusion coefficient (*D*) is adjusted for the increased viscosity; when *D* is not adjusted *D* for the reference condition (water at 37 °C, level 1 viscosity) is used

level 1 viscosity, the simulated particle motion suggested negative (downward) motion for the 200 μm diameter particles at all periods of the pulse at 8 mL $min^{-1}$, whereas at 16 mL $min^{-1}$ some positive (upward) motion was simulated (Fig. 4a *vs* b). In the level 3 viscosity medium, both positive and negative velocities were observed, but higher positive velocity, implying more upward motion than downward at both flow rates (Fig. 4c *vs* d).

Figure 4a (level 1 viscosity, 8 mL $min^{-1}$), therefore, illustrates a relatively high particle velocity in the downward direction; however, the particle will not, in reality, continue indefinitely downwards, and will eventually rest at the base of the cell. Similarly, Fig. 4d (level 3 viscosity, 16 mL $min^{-1}$) shows a higher overall upward particle velocity, nonetheless the particle will not continue indefinitely upwards, but would be halted at the top of the cell.

In situations where particles are not moving, with motion halted by the spatial limitations of the top or base of the cell, the dissolution simulation can be set such that particle motion is disabled, and the Re is calculated based on absolute fluid velocity.

### *Effect of Absolute Velocity (Particle Motion Disabled)*

From Fig. 5, it is clear that using absolute fluid velocity at 16 mL $min^{-1}$ (disabling particle motion) for the larger 200 μm particles, decreased the simulated dissolution rate in the level 1 viscosity medium, as the fluid velocity relative to a particle (now with zero motion) was less than when particle motion was enabled, and the simulated dissolution rate was reduced. On the contrary, for the example of level 3 viscosity where relative velocity was low when particle motion was enabled (*e.g.* Fig. 4d), by disabling particle motion the velocity relative to the particle, and thus the simulated dissolution rate, was increased. The effect of enabling or disabling particle motion on dissolution therefore depends on whether the relative velocity is greater or less than the absolute velocity in any dissolving medium-particle system, which in turn is affected by particle size and fluid viscosity. When D is adjusted for viscosity, the effect of viscosity on diffusion dominates over particle motion/hydrodynamic effects.

### *Identifying Particle Suspension Behaviour*

Figure 6 shows particle motion of 200 μm particles at 8 mL $min^{-1}$ in level 2 viscosity. Velocity data taken from the first 10 s illustrate that initially the particle motion was predominantly negative. However, as the particle diameter reduces, there was less negative particle velocity, and examining the motion of the dissolving particle over 2 h (Fig. 6b) it is clear that the particles had both positive and negative motion, suggesting that they are likely to be retained in suspension. This simulation is supported by observed data. When CBZ (particle size d50 262 μm) was subject to a dissolution test in media approximating level 1 (water) and level 2 (0.3% *w/v* HPMC; viscosity 1.37 mPa.s) at 8 mL $min^{-1}$,

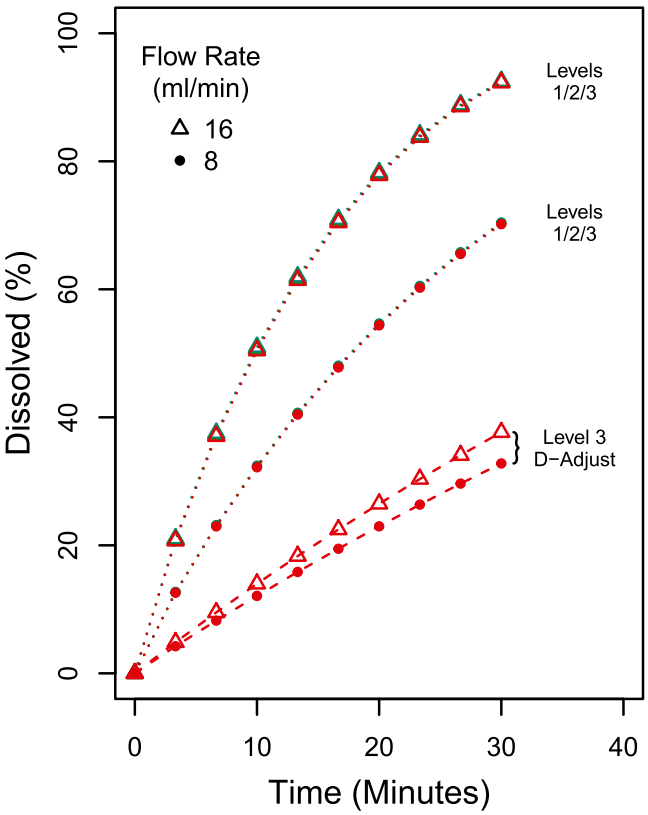


**Fig. 3.** Effect of viscosity and flow rate on simulated dissolution of 20 μm diameter particles, solubility 0.23 mg $mL^{-1}$. Levels 1–3 refer to viscosity 0.7 mPa.s, 1.4 mPa.s and 12.3 mPa.s respectively. *D*-adjust refers to the simulated dissolution profile when the diffusion coefficient (*D*) is adjusted for the increased viscosity; when *D* is not adjusted *D* for the reference condition (water at 37 °C, level 1 viscosity) is used

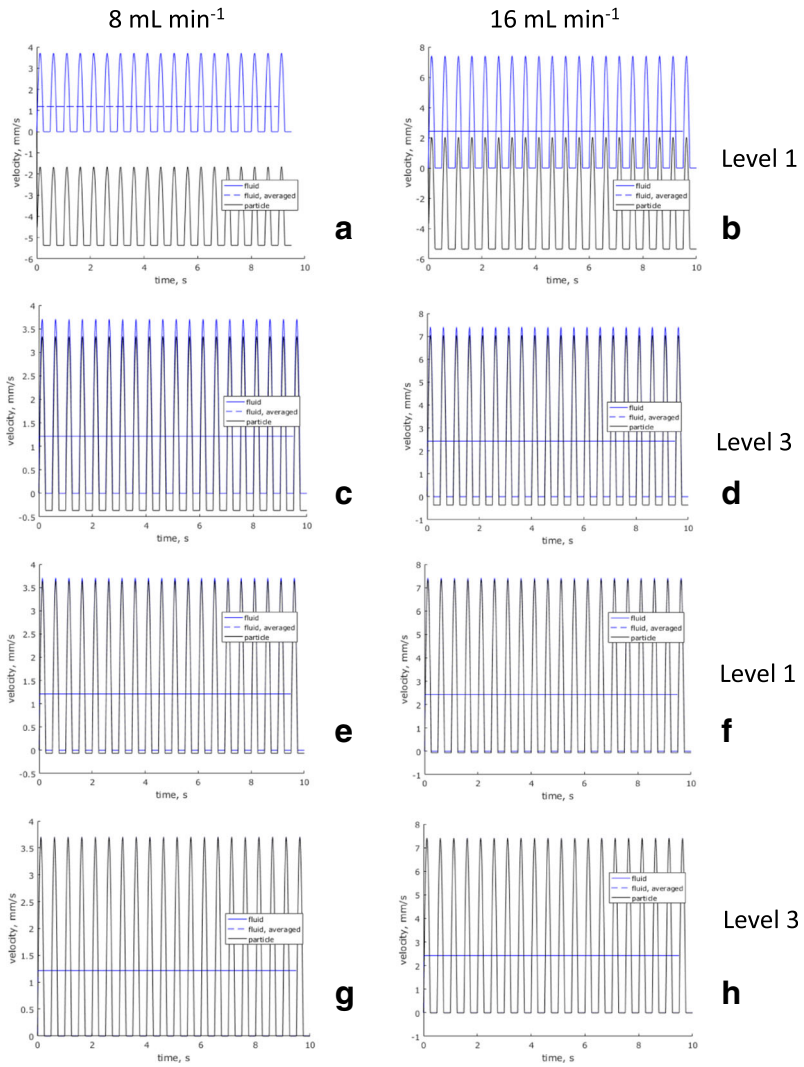


**Fig. 4.** Simulated particle and fluid velocities over first 10 s of simulation, solubility 0.23 mg $mL^{-1}$: **a-d** 200 μm diameter particles, E–H 20 μm diameter particles. **a**: 8 mL $min^{-1}$, **b**: 16 mL $min^{-1}$, level 1 viscosity; **c**: 8 mL $min^{-1}$, **d**: 16 mL $min^{-1}$, level 3 viscosity; **e**: 8 mL $min^{-1}$, **f**: 16 mL $min^{-1}$, level 1 viscosity; **g**: 8 mL $min^{-1}$, **h**: 16 mL $min^{-1}$, level 3 viscosity. (Pulsating) blue line, fluid velocity; black line, particle velocity; horizontal blue line is average fluid velocity

the particle behaviour was found to be considerably different. In water, the particles mostly remained as a loosely moving bed at the base of the cell with some particles suspended, while in the HPMC solution more of the CBZ particles were retained in suspension. This is illustrated in the SGI data in Fig. 7, showing the presence of particles suspended in the observation window over 30 min dissolution from each system. The retention of particles in suspension in the more viscous HPMC solution (level 2 viscosity) over the course of the dissolution test is compliant with the suggestions from the simulation model, as is the sedimentation of the particles in water (level 1 viscosity, particle motion similar to Fig. 4a) due to the higher downward particle velocity in this medium.

*Effect of Pulsation and Gravity (Particle Motion Enabled)*

Figure 8 illustrates that, for the 200 μm particles with gravity enabled, there was little difference between simulated dissolution based on flow modality (i.e. in a pulsing *vs.* constant flow), but the effect of gravity was significant. In the absence of gravitational acceleration, the overall dissolution rate was much lower. Furthermore, for the constant flow case, there was no effect on simulated dissolution profiles from altering viscosity (*D* unadjusted) when gravity was disabled (data not shown).

Conversely, for the smaller 20 μm particles there was little effect from either gravity or pulse on the overall dissolution rate (data not shown), with the simulated dissolution profiles being very similar to those in Fig. 3 (*D* unadjusted).

The particle and fluid velocity plots in Fig. 9 illustrate the minimal relative velocity attained by the particle motion in the absence of gravitational acceleration for the 200 μm particles, for either pulsing or constant flow. When gravitational effects were included in the simulation, the relative velocity magnitude was similar with and without the pulse (Fig. 9c/Fig. 4a).

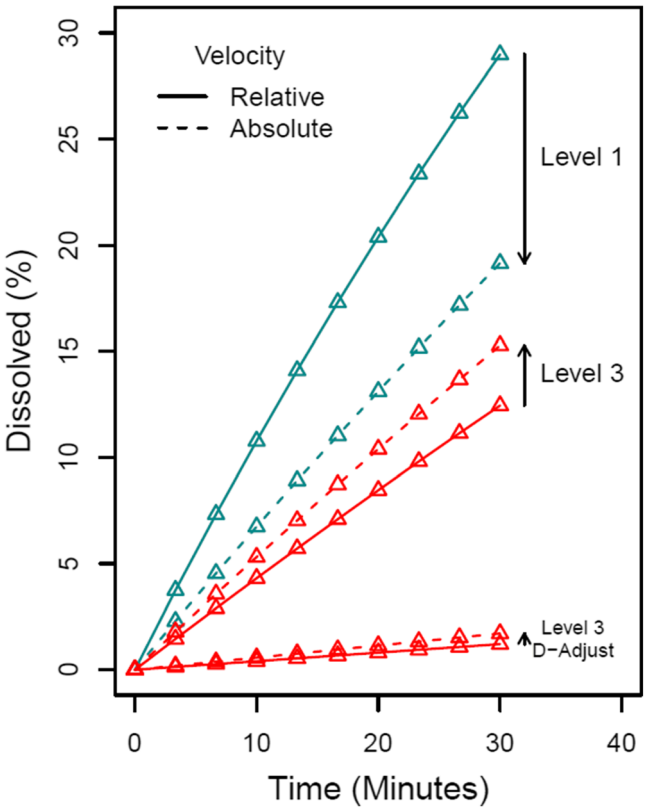


**Fig. 5.** Effect of disabling particle motion (absolute velocity) and enabling particle motion (relative velocity) on simulated dissolution of 200 μm diameter particles, solubility 0.23 mg $mL^{-1}$, at 16 mL $min^{-1}$. Levels 1 and 3 refer to viscosity level 1 (0.7 mPa.s) and level 3 (12.3 mPa.s). *D*-adjust refers to the simulated dissolution profile when the diffusion coefficient (*D*) is adjusted for the increased viscosity; when *D* is not adjusted *D* for the reference condition (water at 37 °C, level 1 viscosity) is used

In summary, for the flow through apparatus, incorporating the effect of gravity notably affected the simulated dissolution results of the larger 200 μm particles but not the 20 μm particles with particle motion enabled, but flow pulsation had little effect.

## Paddle Apparatus

### *Effect of Viscosity and Flow Velocity on Simulated Dissolution in the Paddle Apparatus*

Dissolution in the paddle apparatus simulations were in zero-gravity conditions, with constant flow and 900 mL dissolution medium. Based on the results from the flow through apparatus, it was expected that disabling gravity and using a constant flow would result in the viscosity values (*D* unadjusted) used having a negligible effect on the simulated dissolution rate. Simulated dissolution rates of the 200 μm diameter particles in the paddle apparatus are presented in Fig. 10a. As expected, neither the effect of velocity or viscosity (*D* unadjusted) impacted notably on the simulated dissolution rate over 30 min (< 10% dissolved), whereas molecular diffusion (*D* adjusted) clearly affected the simulated dissolution. Simulated dissolution from the 20 μm diameter particles suggested 100% dissolution in 16 min (0.0024 m $s^{-1}$) (data not shown). When comparing dissolution simulations in the flow through and paddle apparatuses, an analogous case in the flow through apparatus is a constant flow field with gravity disabled, at 16 mL $min^{-1}$ (0.0024 $ms^{-1}$, (Table II)), level 1 viscosity. In this situation, conditions are the same as those used in the lower velocity paddle apparatus simulations, except for reservoir and cell volumes affecting simulated local concentrations. The simulated dissolution in the flow through apparatus was slower for the 20 μm diameter particles, with 69% dissolved at 16 min (compared to 100% in paddle apparatus) and 92% dissolved at 30 min.

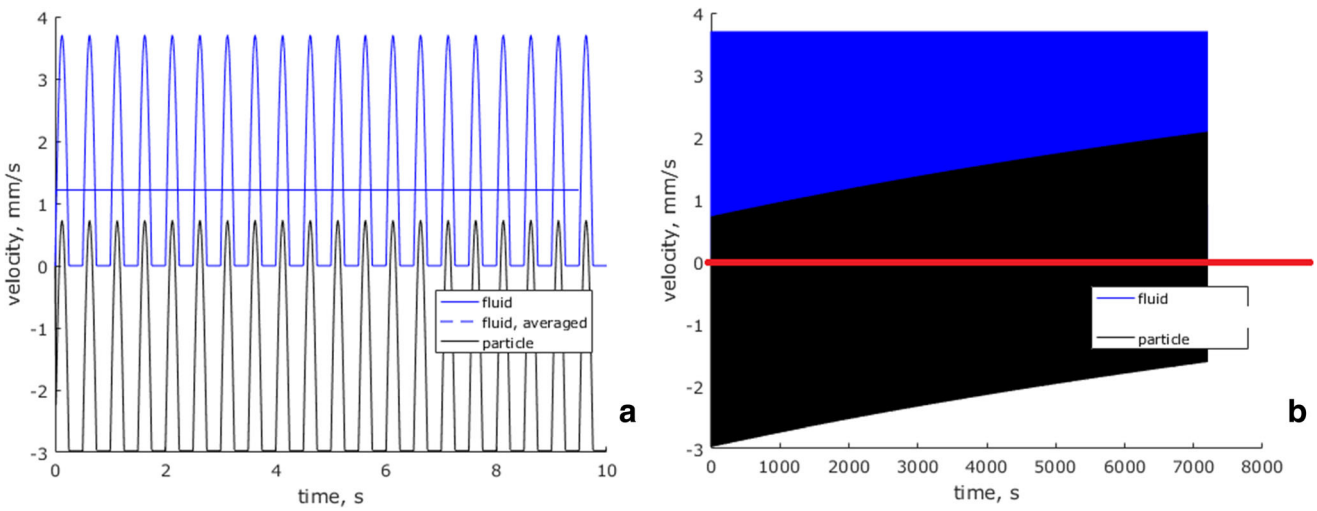


**Fig. 6.** Particle (200 μm diameter, solubility 0.23 mg $mL^{-1}$) and fluid motion at 8 mL $min^{-1}$, level 2 viscosity, for **a**: 10 s and **b**: 2 h (red line highlights zero velocity, at the transition between upward and downward motion). This figure (**b**) represents pulsing particle and fluid motion; however, the pulsing particle and fluid profiles visible in this figure (**a**) appear as a block of colour in this figure (**b**), due to the condensed time baseline in the image in panel **b**. Blue line, fluid velocity; black line, particle velocity; horizontal blue line in this figure (**a**) is average fluid velocity

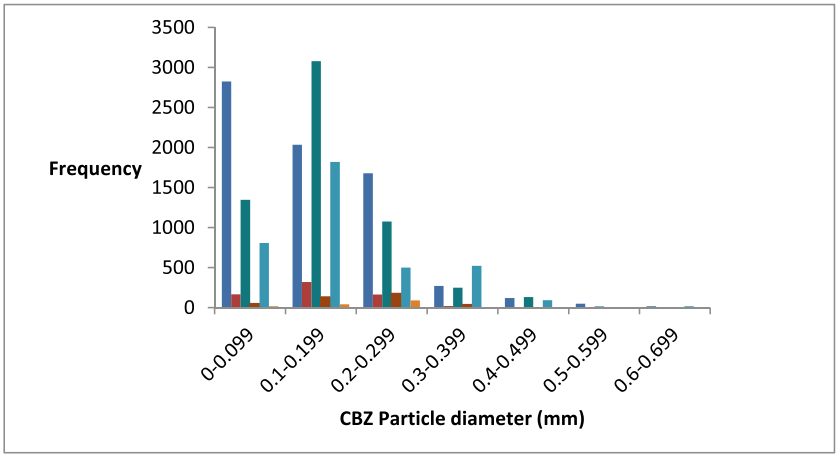


**Fig. 7.** CBZ particle size and frequency of suspended particles captured in the SGI visualisation region of the cell (cell mid-section), over the 15 s of SGI analysis at each time point, from 10 to 30 min in 0.3% *w/v* HPMC solution (1.37 mPa.s) and degassed water (0.7 mPa.s); 8 mL $min^{-1}$ flow through dissolution apparatus. ● HPMC solution 10 min; ● HPMC solution 20 min; ● HPMC solution 30 min; ● Water 10 min; ● Water 20 min; ● Water 30 min

*Simulated Particle and Fluid Velocities*

The particle velocity increased with increased fluid velocity, but in each case was similar to the fluid velocity (Fig. 10b, c) in the paddle apparatus, resulting in the low relative velocity.

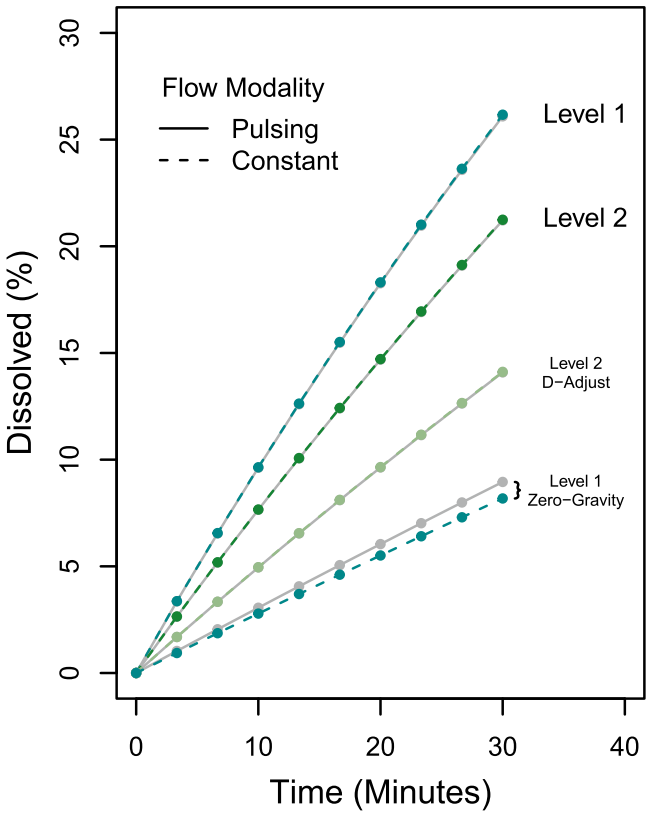


**Fig. 8.** Effect of pulse and gravity on simulated dissolution of 200 μm diameter particles, solubility 0.23 mg $mL^{-1}$, at 8 mL $min^{-1}$. Levels 1–2 refer to viscosity 0.7 mPa.s and 1.4 mPa.s respectively. *D*-adjust refers to the simulated dissolution profile when the diffusion coefficient (*D*) is adjusted for the increased viscosity; when *D* is not adjusted *D* for the reference condition (water at 37 °C, level 1 viscosity) is used. Continuous and pulsing profiles are superimposed except under zero-gravity conditions

## DISCUSSION

### Particle Motion Effects

The role of viscosity on tablet disintegration and/or dissolution has been explored from a number of perspectives (22,37–43), with an increase in viscosity generally being associated with a reduction in tablet disintegration, particularly when reduced water diffusivity in more viscous media was observed. The results presented here illustrate the mechanistic effects of small increases in medium viscosity on dissolution of particulate systems—*i.e.* dissolution of active ingredient only or dissolution post-disintegration. The effect of viscosity on particle motion, especially larger particles, and consequent impact on dissolution even when *D* is unaffected is highlighted. An increase in viscosity is anticipated to reduce dissolution due to a decrease in relative particle motion and Re. However, reduced particle motion, under certain combined conditions of flow velocity, viscosity and particle size, can result in the particles remaining suspended rather than sedimenting to the cell base or floating to the top. Sedimentation can lead to formation of a powder bed/cone with consequent reduction of exposed surface area and local concentration gradients, negatively impacting the dissolution rate. The observed example presented in the SGI images in the current work illustrates two very different particulate systems: one retained in suspension throughout the cell and the other tending to locate near the base of the cell, with the difference in behaviour in these systems resulting from just a small increase in viscosity, equivalent of water to milk at 37 °C. As the solubility of CBZ is higher in HPMC solution than water (44), the difference in dissolution for the same CBZ particulate system in the same flow through apparatus dissolution conditions, could erroneously be attributed to

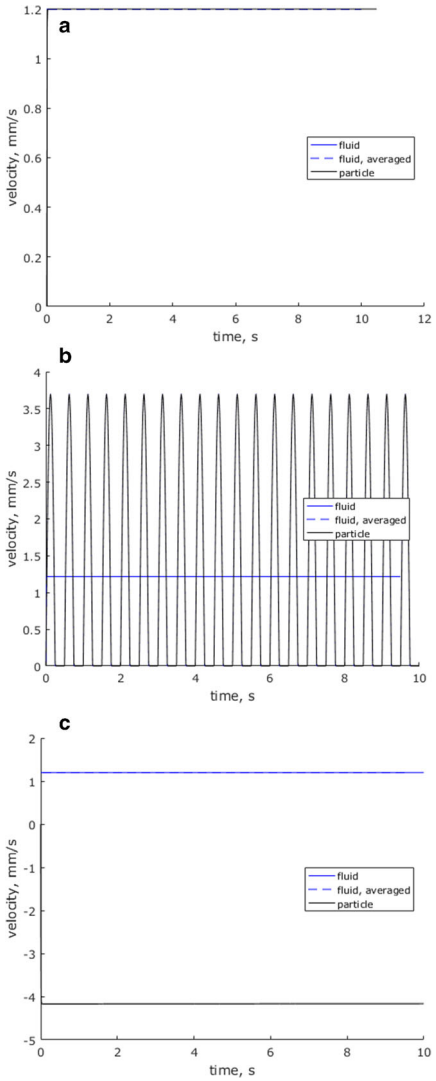


**Fig. 9.** 200 μm diameter particle and fluid velocity over first 10 s of simulation, at 8 mL $min^{-1}$, level 1 viscosity **a**: constant flow zero gravity; **b**: pulsing flow zero gravity; **c**: with gravity constant flow. Blue line, fluid velocity; black line, particle velocity (particle and fluid velocity profiles are superimposed in this figure (**a** and **b**). Horizontal blue line in this figure (**b**) is average fluid velocity

medium solubility effects alone. The current work demonstrates the value of the additional insight, from dissolution simulation and imaging, into viscosity-mediated changes in particulate behaviour during dissolution testing in media of differing viscosity.

## Simulation Limitations and Potential

The simulated effect of flow rate on dissolution, when particle motion was enabled, was particularly evident for the simulated dissolution of the smaller 20 μm particles. As the relative velocity values were very low for these smaller particles, the effect of flow rate on concentration local to the dissolving particle mediated the simulated effect on dissolution. The inlet medium from the reservoir has a lower concentration than the local bulk medium; therefore, a higher flow rate essentially 'flushes' the inlet medium through at a faster rate, leading to simulation of a higher local concentration gradient. It is unlikely in reality that a situation can arise where flow rates notably affect the concentration at the dissolving surface when relative velocity approximates zero; rather, the simulated results suggest whether relative particle velocity or flow rate effects on the local concentration gradient might dominate observed results. These results highlight the importance, especially for smaller particles, of considering local volume and fluid flow rates, both in the observed apparatus and as defined in the simulation.

Flow along one axis only is simulated in the current work, since the model does not simulate a 2- or 3-D hydrodynamic environment. Nonetheless, in the case of this lumped parameter unidirectional simulation, simulated particulate behaviour can facilitate selection of the most appropriate particle motion status (enabled or disabled) to approximate the behaviour of the system in the dissolution environment. This selection could be further refined according to particle size distribution (particle motion enabled for smaller particles and disabled for larger) and time (as the larger particle dissolves motion could be enabled upon reaching a threshold value). In this manner, a more realistic particle motion environment can be captured through exploitation of the particle motion option for a particular particulate system. However, if all particles tend towards one of the cell boundaries there are likely to be additional inter-particulate effects on local concentration gradients.

A consequence of the limitation of a unidirectional flow profile is that gravitational effects can only be included when the flow profile is in the same dimension as gravitational acceleration. Contrary to the situation with vertical flow in the flow through apparatus, simulation of dissolution in the paddle apparatus excludes gravitational effects due to the primary direction of flow being rotational about the vertical axis. As described, for smaller particles in suspension, enabling gravity had no observable effect on the simulated dissolution rate, with the main effect on simulated dissolution being from variation in $D$. Comprehensive replication of all of the complex mechanistic effects of the hydrodynamic environment on dissolution in the paddle apparatus, including axial and radial velocities and centrifugal forces, would require a full 3D simulation, and there is likely to be an influence from gravity in particular in lower velocity regions.

The effect of agitation rate (*via* paddle rotation speed) on coning potential in the low velocity region in the centre of the vessel base has been investigated for both viscous and non-viscous fluids (associated with laminar and turbulent flow, respectively, based on the Reynolds numbers attained) (45,46), using a form of the Zwietering equation. The results suggested mechanistic differences in coning phenomena in viscous *vs* non-viscous fluids, likely relating to countering effects of viscosity. An increased viscosity will both aid particle suspension and reduce coning potential, but also hinder momentum transfer from increased rotation of the paddle, reducing local velocity and increasing coning potential. Thus, a small increase in medium viscosity is likely to reduce cone formation *via* sedimentation, as long as local velocities are sufficient for particulate suspension to take place.

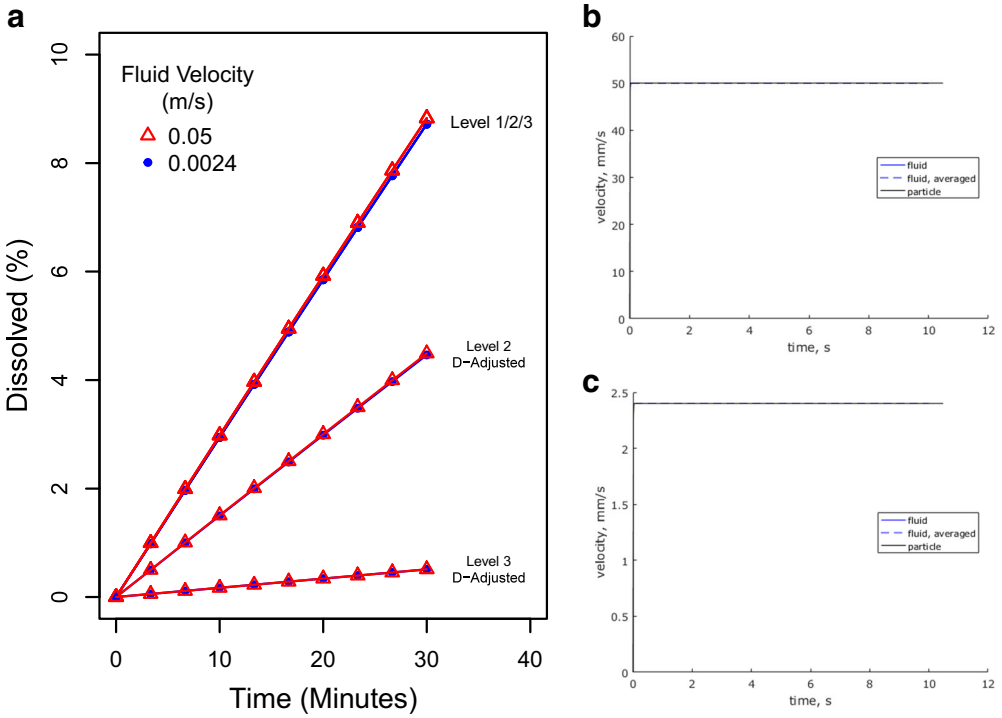


**Fig. 10.** **a**: Effect of fluid velocity and viscosity on simulated dissolution of 200 μm diameter particles, solubility 0.23 mg $mL^{-1}$, in the paddle apparatus. Levels 1–3 refer to viscosity 0.7 mPa.s, 1.4 mPa.s and 12.3 mPa.s respectively. *D*-adjusted refers to the simulated dissolution profile when the diffusion coefficient (*D*) is adjusted for the increased viscosity; when D is not adjusted D for the reference condition (water at 37 °C, level 1 viscosity) is used. **b-c**: particle and fluid velocities over first 10 s of simulation; at **b**: 0.05 m $s^{-1}$ and **c**: 0.0024 m $s^{-1}$. Blue line, fluid velocity; black line, particle velocity; (particle and fluid velocity profiles are superimposed in this figure **b** and **c**).

The simulations presented in this work employ a single value for the inputs used, and the topic of simulating variability has not been presented. Variability could be represented by, for example, a particle size distribution rather than one particle size value, as previously illustrated (26); the execution of batch simulations which include a frequency distribution of data (*e.g.* variation of solubility with pH, based on a frequency distribution of physiological pH values); or use of Monte Carlo simulations to simulate variability from an input data set.

## CONCLUSION

Whereas viscosity is proposed as a medium property whose effect on dissolution is addressed in the most complex media, incidental changes in medium viscosity, consequent to gastric fed state medium composition in particular, could affect the dissolution rate. Effects of viscosity on dissolution include reduced molecular diffusion, reduced relative particle velocity, and the potential to retain particulate systems in suspension. The dissolution simulation options presented enable interpretation of these effects of viscosity. A limitation of the lumped parameter, unidirectional simulation approach is the negation of gravitational acceleration when flow direction is not vertical, and of a spatially resolved hydrodynamic field—factors which are likely to be less influential for smaller particles. The range of simulated situations presented in the current work illustrates the potential of *in silico* dissolution simulation, which can be expanded to include sources of variability in the simulation. In conclusion, IPD testing should include an understanding of the impact of relatively small changes in dissolution medium viscosity on dissolution results obtained. *In silico* predictions using the fluid dynamics model can assist in this endeavour, and are optimally employed when a thorough understanding of the benefits and limitations of the simulation model are clarified.



## REFERENCES

1. Todaro V, Persoons T, Grove G, Healy AM, D'Arcy DM. Characterization and simulation of hydrodynamics in the paddle, basket and flow-through dissolution testing apparatuses-a review. Dissolut Technol. 2017;24(3):24–36.
2. Markopoulos C, Andreas CJ, Vertzoni M, Dressman J, Reppas C. In-vitro simulation of luminal conditions for evaluation of performance of oral drug products: choosing the appropriate test media. Eur J Pharm Biopharm. 2015;93:173–82.
3. Maharaj AR, Edginton AN, Fotaki N. Assessment of age-related changes in pediatric gastrointestinal solubility. Pharm Res. 2016;33(1):52–71. https://doi.org/10.1007/s11095-015-1762-7.
4. Kostewicz ES, Abrahamsson B, Brewster M, Brouwers J, Butler J, Carlert S, *et al.* In vitro models for the prediction of in vivo performance of oral dosage forms. Eur J Pharm Sci. 2014;57:342–66. https://doi.org/10.1016/j.ejps.2013.08.024.

5. McAllister M. Dynamic dissolution: a step closer to predictive dissolution testing? Mol Pharm. 2010;7(5):1374–87. https://doi.org/10.1021/mp1001203.
6. Pedersen PB, Vilmann P, Bar-Shalom D, Müllertz A, Baldursdottir S. Characterization of fasted human gastric fluid for relevant rheological parameters and gastric lipase activities. Eur J Pharm Biopharm. 2013;85(3):958–65.
7. Reppas C, Karatza E, Goumas C, Markopoulos C, Vertzoni M. Characterization of contents of distal ileum and cecum to which drugs/drug products are exposed during bioavailability/bioequivalence studies in healthy adults. Pharm Res. 2015;32(10):3338–49. https://doi.org/10.1007/s11095-015-1710-6.
8. Jantratid E, Janssen N, Reppas C, Dressman JB. Dissolution media simulating conditions in the proximal human gastrointestinal tract: an update. Pharm Res. 2008;25(7):1663–76. https://doi.org/10.1007/s11095-008-9569-4.
9. Garbacz G, Cadé D, Benameur H, Weitschies W. Bio-relevant dissolution testing of hard capsules prepared from different shell materials using the dynamic open flow through test apparatus. Eur J Pharm Sci. 2014;57:264–72.
10. Sun W, Houghton LA, Read N, Grundy D, Johnson A. Effect of meal temperature on gastric emptying of liquids in man. Gut. 1988;29(3):302–5.
11. Koziolek M, Grimm M, Becker D, Iordanov V, Zou H, Shimizu J, *et al.* Investigation of pH and temperature profiles in the GI tract of fasted human subjects using the Intellicap® system. J Pharm Sci. 2015;104(9):2855–63.
12. Schiller C, Frohlich CP, Giessmann T, Siegmund W, Monnikes H, Hosten N, *et al.* Intestinal fluid volumes and transit of dosage forms as assessed by magnetic resonance imaging. Aliment Pharmacol Ther. 2005;22(10):971–9. https://doi.org/10.1111/j.1365-2036.2005.02683.x.
13. Koziolek M, Schneider F, Grimm M, Modebeta C, Seekamp A, Roustom T, *et al.* Intragastric pH and pressure profiles after intake of the high-caloric, high-fat meal as used for food effect studies. J Control Release. 2015;220(Pt A):71–8. https://doi.org/10.1016/j.jconrel.2015.10.022.
14. Perivilli S, Kakhi M, Stippler E. Computational fluid dynamics simulation of hydrodynamics in USP apparatus 3-the influence of dip rate. Pharm Res. 2015;32(4):1304–15. https://doi.org/10.1007/s11095-014-1534-9.
15. Perivilli S, Prevost R, Stippler E. Velocity field visualization in USP dissolution apparatus 3 using particle image velocimetry. Pharm Res. 2017;34(6):1330–7. https://doi.org/10.1007/s11095-017-2151-1.
16. Pal A, Indireshkumar K, Schwizer W, Abrahamsson B, Fried M, Brasseur JG. Gastric flow and mixing studied using computer simulation. Proc R Soc B. 2004;271(1557):2587–94. https://doi.org/10.1098/rspb.2004.2886.
17. Du P, O'Grady G, Gao J, Sathar S, Cheng LK. Toward the virtual stomach: progress in multiscale modeling of gastric electrophysiology and motility. Wiley Interdiscip Rev Syst Biol Med. 2013;5(4):481–93. https://doi.org/10.1002/wsbm.1218.
18. Du P, Paskaranandavadivel N, Angeli TR, Cheng LK, O'Grady G. The virtual intestine: in silico modeling of small intestinal electrophysiology and motility and the applications. Wiley Interdiscip Rev Syst Biol Med. 2016;8(1):69–85. https://doi.org/10.1002/wsbm.1324.
19. Ferrua MJ, Singh RP. Modeling the fluid dynamics in a human stomach to gain insight of food digestion. J Food Sci. 2010;75(7):R151–62. https://doi.org/10.1111/j.1750-3841.2010.01748.x.
20. Imai Y, Kobayashi I, Ishida S, Ishikawa T, Buist M, Yamaguchi T. Antral recirculation in the stomach during gastric mixing. Am J Phys. 2013;304(5):G536–42. https://doi.org/10.1152/ajpgi.00350.2012.
21. Klein S, Butler J, Hempenstall JM, Reppas C, Dressman JB. Media to simulate the postprandial stomach I. Matching the physicochemical characteristics of standard breakfasts. J Pharm Pharmacol. 2004;56(5):605–10. https://doi.org/10.1211/0022357023367.
22. Radwan A, Wagner M, Amidon GL, Langguth P. Bio-predictive tablet disintegration: effect of water diffusivity, fluid flow, food composition and test conditions. Eur J Pharm Sci. 2014;57:273–9.
23. Korson L, Drost-Hansen W, Millero FJ. Viscosity of water at various temperatures. J Phys Chem. 1969;73(1):34–9.
24. Klein S. The use of biorelevant dissolution media to forecast the in vivo performance of a drug. AAPS J. 2010;12(3):397–406.
25. Sugano K. Theoretical comparison of hydrodynamic diffusion layer models used for dissolution simulation in drug discovery and development. Int J Pharm. 2008;363(1–2):73–7. https://doi.org/10.1016/j.ijpharm.2008.07.002.
26. D'Arcy DM, Persoons T. Mechanistic modelling and mechanistic monitoring: simulation and shadowgraph imaging of particulate dissolution in the flow-through apparatus. J Pharm Sci. 2011;100(3):1102–15. https://doi.org/10.1002/jps.22337.
27. United States Pharmacopoeia 41/National Formulary 36. Rockwell, MD, USA: The United States Pharmacopeial Convention; 2018.
28. Serrano DR, Persoons T, D'Arcy DM, Galiana C, Dea-Ayuela MA, Healy AM. Modelling and shadowgraph imaging of cocrystal dissolution and assessment of in vitro antimicrobial activity for sulfadimidine/4-aminosalicylic acid cocrystals. Eur J Pharm Sci. 2016;89:125–36. https://doi.org/10.1016/j.ejps.2016.04.030.
29. Bird R, Stewart W, Lightfoot E. Transport phenomena. 2nd ed. New York: Wiley; 2002.
30. Kovacevic I, Parojcic J, Homsek I, Tubic-Grozdanis M, Langguth P. Justification of biowaiver for carbamazepine, a low soluble high permeable compound, in solid dosage forms based on IVIVC and gastrointestinal simulation. Mol Pharm. 2009;6(1):40–7. https://doi.org/10.1021/mp800128y.
31. Lee H, Park SA, Sah H. Surfactant effects upon dissolution patterns of carbamazepine immediate release tablet. Arch Pharm Res. 2005;28(1):120–6.
32. Diebold SM, Dressman JB. Hydrodynamik kompendialer Lösungsgeschwindigkeits-Testapparaturen Paddle und Basket. Pharm Ind. 2001;63(1):94–104.
33. Diebold SM. Hydrodynamik und Losungsgeschwindigkeit-Untersuchungen zum Einfluss der Hydrodynamik auf die Losungsgeschindigkeit schwer wasserloslicher Arzneistoffe. Frankfurt am Main. Germany: Johann Wolfgang Goethe Universitat; 2000.
34. D'Arcy DM, Corrigan OI, Healy AM. Hydrodynamic simulation (computational fluid dynamics) of asymmetrically positioned tablets in the paddle dissolution apparatus: impact on dissolution rate and variability. J Pharm Pharmacol. 2005;57:1243–50.
35. D'Arcy DM. Use of computational fluid dynamics to investigate the relationship between hydrodynamics and rates of dissolution. Trinity College Dublin: Dublin; 2007.
36. Anwar S, Fell J, Dickinson P. An investigation of the disintegration of tablets in biorelevant media. Int J Pharm. 2005;290(1–2):121–7.
37. Cvijić S, Parojčić J, Langguth P. Viscosity-mediated negative food effect on oral absorption of poorly-permeable drugs with an absorption window in the proximal intestine: in vitro experimental simulation and computational verification. Eur J Pharm Sci. 2014;61:40–53.
38. Radwan A, Ebert S, Amar A, Münnemann K, Wagner M, Amidon GL, *et al.* Mechanistic understanding of food effects: water diffusivity in gastrointestinal tract is an important parameter for the prediction of disintegration of solid oral dosage forms. Mol Pharm. 2013;10(6):2283–90.
39. Radwan A, Amidon GL, Langguth P. Mechanistic investigation of food effect on disintegration and dissolution of BCS class III compound solid formulations: the importance of viscosity. Biopharm Drug Dispos. 2012;33(7):403–16. https://doi.org/10.1002/bdd.1798.
40. Braun RJ, Parrott EL. Influence of viscosity and solubilization on dissolution rate. J Pharm Sci. 1972;61(2):175–8.

41. Sarisuta N, Parrott EL. Relationship of dissolution rate to viscosity of polymeric solutions. J Pharm Sci. 1982;71(12):1375–80.
42. Nelson K, Shah A. Mass transport in dissolution kinetics I: convective diffusion to assess the role of fluid viscosity under forced flow conditions. J Pharm Sci. 1987;76(10):799–802.
43. Shah A, Nelson K. Mass transport in dissolution kinetics II: convective diffusion to assess role of viscosity under conditions of gravitational flow. J Pharm Sci. 1987;76(12):910–3.
44. Zarmpi P, Flanagan T, Meehan E, Mann J, Fotaki N. Biopharmaceutical understanding of excipient variability: effect of HPMC level and viscosity type on drug solubility. AAPS Annual Meeting; San Diego, USA: http://abstracts.aaps.org/published/; 2017.
45. Higuchi M, Yoshihashi Y, Tarada K, Sugano K. Minimum rotation speed to prevent coning phenomena in compendium paddle dissolution apparatus. Eur J Pharm Sci. 2014;65:74–8. https://doi.org/10.1016/j.ejps.2014.09.010.
46. Higuchi M, Terada K, Sugano K. Coning phenomena under laminar flow. Eur J Pharm Sci. 2015;80:53–5.